Journal of Energy Storage 64 (2023) 107100

Contents lists available at ScienceDirect

Journal of Energy Storage

journal homepage: www.elsevier.com/locate/est

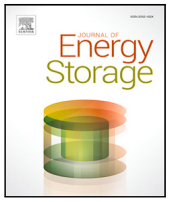

Research papers

Community energy storage system: Deep learning based optimal energy management solution for residential community

Md. Morshed Alam, Raihan Bin Mofidul, Yeong Min Jang *

Department of Electronics Engineering, Kookmin University, Seoul, South Korea

ARTICLE INFO

Keywords:
Energy management system
Community energy storage system
Optimal scheduling
Optimization algorithm
Bi-directional long short-term memory
Clustering algorithm

ABSTRACT

The concept of community energy storage system (CESS) is required for the efficient and reliable utilization of renewable energy and flexible energy sharing among consumers. This paper proposes a novel approach to assess the practical benefits of CESS deployment in a residential community by decreasing the daily electricity cost and maximizing the self-consumption of PV energy. To this end, a deep-learning-based forecasting model, namely a bi-directional long short-term memory model, is implemented to predict the operational constraints and dependency. Furthermore, a hybrid optimization technique that comprises a clustering and optimization algorithm is developed in which the clustering algorithm ensures appropriate combinations of user groups to develop optimal control policies. Finally, the forecasting model is integrated with the hybrid optimization algorithm to find the optimal solution involving PV-CESS energy utilization. Numerical analyses are performed using real historic data of the energy demand and PV generation for three consecutive days considering different scenarios. The results demonstrate that the electricity costs and self-consumption associated with the CESS are lower and greater than those of an individual ESS system, respectively, with the daily electricity cost decreasing by 21.89%, 13.81%, and 7.66% in the three analyzed scenarios.

1. Introduction

An energy crisis is being encountered worldwide owing to global political unrest and the significant demand for nonrenewable energy. Additionally, global warming is intensifying because of the massive usage of nonrenewable energy. The challenges associated with the energy crisis and corresponding environmental issues can be mitigated by ensuring the high penetration and proper utilization of renewable energy sources (RESs) [1]. To optimize the utilization, artificial intelligence technologies must be integrated. Moreover, the flexibility and quality of RES systems must be enhanced. Recently, subsidies have been offered for building integrated PV panels for increasing the penetration of PV systems in residential areas [2]. In addition, utility companies are encouraging consumers to participate in demand response programs to reduce their electricity bills. To ensure that residential communities can benefit from the integration of photovoltaic (PV) panels with an energy storage system (ESS), PV-community ESSs (CESSs) with optimal capacities and settings must be successfully installed. In addition, proper control and operation strategies must be identified.

Consequently, several researchers have proposed different strategies and models to assess the practical advantages of CESS [3–6]. The techniques used commonly to minimize the electricity cost and carbon emissions include demand load shifting [3], PV energy time shifting [4], combined demand load and PV energy shifting [5], demand load shifting based on peak and low tariff (dynamic tariff), and demand response programs [6]. Recently, many researchers have focused on the use of CESS for energy sharing in a residential community to exploit the advantages of varying load demands and renewable energy generation. Walker et al. analyzed the practical advantages of shared ESS over individual ESS by considering the demand shifting strategy and dynamic tariff for cost calculation [5]. Similarly, Stelt et al. attempted to minimize the grid electricity cost through demand response programs for improving the technical and economic benefits of CESSs [6]. A profit-sharing mechanism was established by sharing power profiles for ensuring the cooperation between a CESS and prosumers [7]. By implementing the operational constraints of a CESS, stochastic PV power generation, and time-varying load, Zhu and Ouahada proposed a distributed sharing control algorithm for promoting the use of RESs and decreasing the cost of energy generation [8]. To decrease the electricity cost during peak tariff, an energy management scheme was developed, in which the utilization of excess PV energy was increased, and the energy credits were distributed among the prosumers [9]. To enable virtual energy sharing among a group of users, a two-stage optimization

* Corresponding author.
E-mail addresses: mmorshed@ieee.org (Md.M. Alam), raihanbinmofidul@ieee.org (R. Bin Mofidul), yjang@kookmin.ac.kr (Y.M. Jang).
URL: http://wireless.kookmin.ac.kr/?page_id=12 (Y.M. Jang).

https://doi.org/10.1016/j.est.2023.107100
Received 26 October 2022; Received in revised form 14 February 2023; Accepted 7 March 2023
Available online 27 March 2023

Nomenclature

$\hat{E}^{CESS}_{max,SOE}$	Maximum SOE of CESS
η^{CESS}_{CF}	CESS capacity factor
$\eta^{H_h,max}_{DF}$	Maximum demand factor
$\eta^{H_h,min}_{DF}$	Minimum demand factor
η^{CESS}_{DOD}	Depth of discharge factor
η^{CESS}_{eff}	CESS efficiency factor
η^{PV}_{eff}	PV system efficiency factor
$\eta^{PV,max}_{GF}$	Maximum generation factor
η^{PV}_{GP}	Average generation periods
η_{opt}	Optimization factor
$\hat{E}^{grid,H_h}_{d,Th_i}$	Set of daily grid energy allowance for houses
$\hat{E}^{CESS}_{d,Cap}$	CESS capacity
$\hat{E}^{PV,G}_{d,Cap}$	PV system capacity
$\hat{E}^{CESS}_{DisA}$	Discharge amount of CESS
$\hat{E}^{H_h}_{D}$	Energy demand of house
$\hat{E}^{H_h,G}_{FD,sum,da}$	Sum of day-ahead forecasted demand during generation
$\hat{E}^{H_h}_{FD,sum,da}$	Sum of day-ahead forecasted demand
$\hat{E}^{H_h,G}_{FD,sum,d}$	Sum of present day forecasted demand during generation
$\hat{E}^{H_h,NG}_{FD,sum,d}$	Sum of present day forecasted demand during no generation
$\hat{E}^{H_h}_{FD,sum,d}$	Sum of present day forecasted demand
$\hat{E}^{H_h}_{FD}$	Forecasted energy demand of house
$\hat{E}^{PV,G}_{FG,sum,da}$	Sum of day-ahead forecasted PV generation
$\hat{E}^{PV,G}_{FG,sum,d}$	Sum of present day forecasted PV generation
$\hat{E}^{PV}_{FG}$	Forecasted PV generation
$\hat{E}^{CESS}_{Fin,SOE}$	Final SOE of CESS
$\hat{E}^{CESS}_{Fin,uses}$	Final usable energy from CESS
$\hat{E}^{H,min}_{I^{PV,G}_{step,d},d}$	Sum of minimum demand during PV generation
$\hat{E}^{CESS}_{Ini,20\%}$	Initial 20% SOE of CESS
$\hat{E}^{CESS}_{Ini,SOE}$	Initial SOE of CESS
$\hat{E}^{grid,H_h}_{m,Th_i}$	Set of monthly grid energy allowance for houses
$\hat{E}^{CESS}_{min,SOE}$	Minimum SOE of CESS
$\hat{E}^{CESS}_{nd,PV}$	Energy needed for charging CESS completely
$\hat{E}^{CESS}_{Pri,SOE}$	Previous day SOE of CESS
$\hat{E}^{H_h,max}_{sum,d}$	Sum of maximum demand of a house
$\hat{E}^{PV,max}_{sum,G}$	Sum of maximum PV generation
$\hat{E}^{PV,G}_{sur}$	Surplus PV generation
A	Set of appliances
H	Set of house
I	Set of time step
PV	Set of PV system
τ	Interval in terms time unit
$\xi^{M_i}_{PV}(t)$	On/off status of PV module at time t
$E^{PV,M_i}_{G,rated}$	Rated capacity of PV panel
$E^{PV}_{G,t}$	PV power generation
$F(x)$	Optimizer function
$G_{PV}(t)$	Solar irradiance at time t
G^{std}_{PV}	Standard solar irradiance
G^{th}_{PV}	Solar irradiance threshold
$I_{step,da}$	Set of time step for following day
$I_{step,d}$	Set of time step for ongoing day
lb	Lower bound
lr	Learning rate
N_a	Number of appliances
N_{cess}	Number of CESS
N_c	Number of cluster
N^h_c	Number of houses in a cluster
N_{day}	Number of days in a month
N_h	Number of houses
$N_{pv,m}$	Number of PV module in a systems
N_{pv}	Number of PV systems
T	Set of time
t_{end}	Set of end period
T_{hr}	Set of time in hour
T_{mnt}	Set of time in minute
$t_{nG,da}$	Set of no generation period on following day
$t_{nG,d}$	Set of no generation period on ongoing day
T_{snd}	Set of time in second
t_{srt}	set of start period
$T^H_{t,d}$	Value of tariff at time t
ub	Upper bound

model was developed based on the electricity price [10]. Jo and Park proposed an energy capacity trading and operation game based scheme for reducing the electricity cost of shared ESS, in which the agent performed capacity trading and 24-h scheduling [11]. Additionally [12], a business model for residential shared ESS was developed based on the interaction between the marginal-cost-based electricity price and elastic demands. An energy sharing model was established for sharing both electrical and thermal energy storage systems [13]. To promote renewable energy utilization and electricity price arbitrage, an energy sharing model was also established in [14]. Liu et al. present a multi-time scale energy purchase model with optimum planning for shared ESS, as well as a cost–benefit analysis, in order to reduce the power procurement costs of electricity retailers [15]. In addition, a day-ahead operation optimization approach is proposed for building-level ESS based on the features of peak-shaving and valley-filling of energy storage, taking into account load fluctuations and real-time electricity prices [16]. Telaretti et al. presented a pricing model for customer-sited energy storage in the context of hourly real-time electricity prices in an attempt to maximize storage owners' profits [17].

However, a contour-based analysis is proposed for improving self-sufficiency and self-consumption of a PV-battery system where the impact of array power and rated capacity of the battery is considered as main indices [18]. Through the assessment of the techno-economic performance and optimal sizing and scheduling of PV system, frequency containment reserve and self-consumption/sufficiency of the PV-battery integrated system are improved in [19,20]. Moreover, Gallego-Castillo et al. analyzed an optimal self-consumption installation under a framework which leads economic savings for self-consumer for both without and with remuneration for energy surplus [21]. However, the impact of sizing of PV and battery in a renewable energy community on electric distribution grid are analyzed and investigated in [22]. Nevertheless, the improvement of self-consumption, self-sufficiency, and sizing of PV-battery are being assessed, it has not considered predictive constraints-based historic data driven approach for finding the optimal solution.

At present, models integrating deep learning and optimization algorithms are being widely incorporated in energy management systems. In such frameworks, deep learning models are typically used as day-ahead forecasting models. Certain researchers developed a scheduling algorithm for hybrid ESSs based on day-ahead predictions. Varzaneh et al. proposed an energy management system to maximize economic profitability by optimizing energy availability for selling to the grid, while using weighted moving average and linear approximation to reduce the difference between forecasted and actual values [23]. To ensure optimal PV-CESS energy sharing among users, an integrated framework was designed and developed [24], with the energy consumption and generation forecasted through a deep learning model. Choi et al. developed a mixed-integer linear programming based cost-optimal scheduling for PV integrated battery ESS, while RNN and CNN are leveraged to reduce the difference between its open-loop training and closed-loop test dynamics [25]. In addition, an ESS integrated microgrid (i.e., an off-grid system) utilizes a predictive management method based on mixed integer linear programming to reduce fuel consumption [26]. A bidirectional long short term memory (Bi-LSTM) model is used to drive the day-ahead constraints for optimal energy management in a PV-ESS integrated house in [27]. Furthermore, a primary technique for distributed optimization, the alternating direction multiplier method (ADMM)-based day-ahead scheduling technique was applied for low-voltage grids and prosumers [28]. Considering a community microgrid, certain researchers [29] introduced ADMM-based peer to peer energy trading and pricing techniques. Iria et al. proposed an ADMM-based bidding optimization technique to coordinate the involvement of prosumers in the day-ahead electricity market [30].

Notably, all the aforementioned studies adopted different optimization methods based on dynamic tariff, time of use tariff, load shifting, demand response program, etc. Load shifting, demand shifting, and demand response programs during high and low tariffs are expected to promote the optimization of the electricity cost. Although these optimization techniques can minimize the cost of electricity or enhance the individual energy usage, they partially ensure customer satisfaction in real-world applications owing to the shifting demand or load. In contrast, the proposed system can decrease the daily electricity cost without reducing the user daily satisfaction (i.e., without changing their lifestyle and load or demand). For this reason, the proposed system applies a deep learning model (i.e., Bi-LSTM) for forecasting ahead generation and consumption to identify the patterns and volume of the PV generation and energy demand of each house. Subsequently, the daily total forecasted PV generation and energy demand of each PV system and house are calculated. Similarly, the total forecasted demand during PV generation and no PV generation of each house are calculated. Considering the initial state of energy (SOE), the amount of PV energy required to completely charge the CESS is determined. The surplus PV energy can be used during the generation periods. Subsequently, by applying the clustering and optimization algorithm, the houses are clustered under each PV for maximizing the surplus PV energy distribution among them in the generation period. During the no generation period, the houses are clustered under each CESS for maximizing the CESS energy distribution. Finally, the grid, PV, and CESS supplied energies to the house are calculated to analyze the cost in the case of individual ESS and CESS.

However, the optimal state of battery charging and discharging is controlled by forecast error and system parameters [31]. For a single residential BESS operation, both PV generation and energy demand forecasting are integrated with a rolling-horizon optimization model [32]. Furthermore, Chapaloglou et al. introduced forecasted load profile classification for desired peak shaving and level smoothing in the power system of an island [33]. In contrast, the proposed system aimed to maximize the use of PV-CESS energy during the absence and presence of PV generation in a residential community. For this reason, this study simulates the integration of a predictive model with an optimization and clustering algorithm that incorporates day-ahead generation and consumption. The main contributions of this study can be summarized as follows:

- A novel hybrid optimization model (i.e., combination of clustering and optimization algorithm) based on the predictive constraints is proposed considering PV-CESS integrated system. The clustering and optimization algorithm ensures the proper energy utilization of the excess PV generation and CESS energy among houses.
- A novel dynamic approach is proposed where each day divides into two operational segments: Operation during PV generation and no PV generation periods. On the eve of every operational period, the proposed algorithm determines the charge and discharge plan for minimizing the daily electricity cost without disrupting the consumer's daily energy usage periods.
- The mathematical formulations for the forecasting model and optimization scheme are developed. The predictive model of the proposed system is used for forecasting the 24 h-ahead PV generation and energy demand to establish the required constraint for the optimal solution.
- The robustness and efficacy of the proposed PV-CESS framework are numerically assessed using three consecutive days of data, considering the daily electricity cost of residential houses and degree of PV energy usage.

The remaining paper is organized as follows: Section 2 presents the mathematical formulation of the proposed system including the forecasting and optimization model. Section 3 introduces the mechanism and various scenarios of the proposed scheme; Section 4 describes the numerical results and model validation. Section 5 presents the concluding remarks and future research directions.

2. System modeling

Consider a grid-connected residential community in which all houses are equipped with PV and ESS systems. The PVs and ESSs are used to supply energy to the houses for decreasing the electricity costs. The proposed scheme replaces this system with a community energy management concept to improve the efficiency and robustness of the system. Fig. 1 shows the proposed energy management architecture of a residential community. Consider that every house has an advanced metering infrastructure system acting as a data provider to the database for storing the historic data of the PV generation and energy demand. The constraints of each house, the CESSs, the PVs, and the forecasted constraints are received as inputs in the optimization model at regular intervals. Additionally, the model receives electricity tariffs under the constraint of the grid energy usage. The output of the cluster and optimization model provides a certain cluster under each PV and CESS and the amount of distributed energy.

This section describes the predictive model for PV and house demand, tariff setting, and properties of PVs and CESSs.

2.1. Forecasting model designing

In [34], Hochreiter and Schmidhuber presented a recursive neural network (RNN) which is known as long short-term memory (LSTM). The intrinsic storage unit and gate mechanism of the LSTM network can address the difficulties of explosion and gradient disappearance existed in RNN, allowing it to preserve delay events in time series and extract them in future training. Fig. 2(a) depicts the LSTM network structure. The mathematical formulation is described as follows [35]:

$$i_t = \sigma\left(\vec{w}_i\left[\vec{h}_{t-1}, x_t\right] + \chi_i\right) \tag{1}$$

$$f_t = \sigma\left(\vec{w}_f\left[\vec{h}_{t-1}, x_t\right] + \chi_f\right) \tag{2}$$

$$o_t = \sigma\left(\vec{w}_o\left[c_t, \vec{h}_{t-1}, x_t\right] + \chi_o\right) \tag{3}$$

$$\vec{h}_t = o_t \cdot tanh(c_t) \tag{4}$$

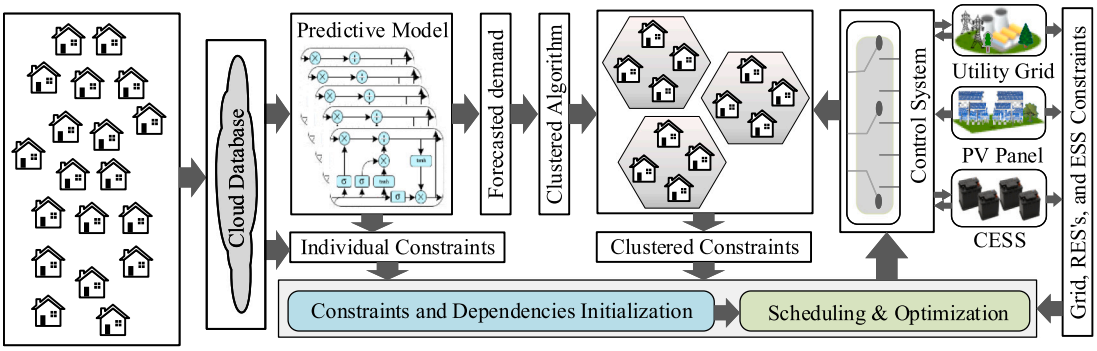

Fig. 1. Proposed intelligent shared energy system architecture.

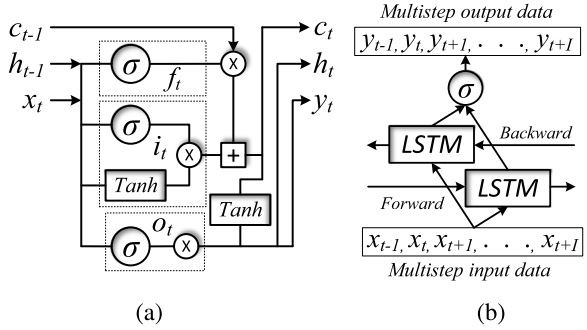

Fig. 2. Network structure of (a) LSTM and (b) Bi-LSTM.

where,

$$c_t = f_t \cdot c_{t-1} + (1 - f_t) \cdot tanh\left(\vec{w}_c \left[\vec{h}_{t-1}, x_t\right] + \chi_c\right) \tag{5}$$

where i_t, f_t, and o_t are the input gate, forget gate, output gate, and c_t is the cell state value. However, the output of each gate depends on the weight matrix (w) and bias term (χ) assigned to it individually. As a consequence, the value of h_t is calculated by from the value of the cell's state and the value of output gate's.

Fig. 2(b) illustrates network architecture of bidirectional learning process that explores both forward and backward sequence directions using two LSTM layers. The following expression computes the output response at time t using a hidden vector produced from two LSTM layers.

$$y_t = \left(LSTM\left(x_t, \vec{h}_{t-1}\right)^{\frown} LSTM\left(x_t, \overleftarrow{h}_{t+1}\right)\right) \tag{6}$$

2.1.1. Forecasted PV power modeling

The performance of the PV power generation system, which transforms solar energy into electrical energy, is highly dependent on solar irradiation. Consequently, the output power of a single module can be expressed as follows:

$$E_{G,t}^{PV,M_i}(t) = \begin{cases} E_{G,rated}^{PV,M_i}\left(\frac{(G_{PV}(t))^2}{G_{PV}^{std} G_{PV}^{th}}\right), G_{PV}(t) \le G_{PV}^{th} \\ E_{G,rated}^{PV,M_i}\left(\frac{G_{PV}(t)}{G_{PV}^{std}}\right), G_{PV}(t) > G_{PV}^{th} \end{cases} \tag{7}$$

$$E_{G,t}^{PV}(t) = \sum_{i=1}^{N_{pv,m}} E_{G,t}^{PV,M_i}(t) * \xi_{PV}^{M_i}(t),\ \xi_{PV}^{M_i}(t) \in [1,0] \tag{8}$$

In the proposed model, we incorporate a PV-CESS integrated system that provides power to houses. Using the actual and predicted generation data, the constraints and dependencies of the PV power generation system are modeled for scheduling the CESS. To this end, the day-ahead PV generation is forecasted by applying the Bi-LSTM model. The mathematical model of the forecasted energy for multi-step output from multi-step input can be described as follows:

$$\begin{aligned} &\left[\hat{E}_{FG,t+1}^{PV}, \hat{E}_{FG,t+2}^{PV}, \ldots, \hat{E}_{FG,t+I_{step}^{PV}}^{PV}\right] = \\ &\prod_{model}^{PV}\left(\left[E_{G,t-T_k+1}^{PV}, \ldots, E_{G,t-1}^{PV}, E_{G,t}^{PV}\right]\right) \\ &\forall t \in T_{hr}, \forall T_{hr} \in T, \forall t \in T_{mnt}, \forall T_{mnt} \in T, \\ &\forall t \in T_{snd}, \forall T_{snd} \in T \end{aligned} \tag{9}$$

where, $\prod_{Model}^{PV}$ represents the Bi-LSTM model for energy demand forecasting and $[I_{step,d}^{PV}, I_{step,da}^{PV}] \in I_{step}^{PV}$. Similarly, $\left[\hat{E}_{FG,t+1}^{PV}, \hat{E}_{FG,t+2}^{PV}, \hat{E}_{FG,t+3}^{PV}, \ldots, \hat{E}_{FG,t+I_{step}^{PV}}^{PV}\right]$ can be determined for $(PV_1, PV_2, PV_3, \ldots, PV_{N_{pv}}) \in \mathbf{PV}$. The starting and ending period of prediction is $[t_{srt,F}, t_{end,F}] \in T$, $t_{srt,F}^{PV} \in t_{srt,F}$, $t_{end,F}^{PV}, \in t_{end,F}$. The total forecasted PV generation in the same day with certain step ahead can be determined as follows:

$$\begin{aligned} &\hat{E}_{FG,sum,d}^{PV,G} = \sum_{j=0}^{I_{step,d}^{PV,G}} \hat{E}_{FG,t}^{PV}(t_{srt,d}^{PV} + j\tau), \\ &\forall I_{step,d}^{PV,G} \in I_{step,d}^{PV}, \forall I_{step,d}^{PV} \in I_{step,d} \end{aligned} \tag{10}$$

where $j = 0$ at t_{srt}^{PV}. The day-ahead total energy demand are calculated as follows:

$$\begin{aligned} &\hat{E}_{FG,sum,da}^{PV,G} = \sum_{j=0}^{I_{step,da}^{PV,G}} \hat{E}_{FG,t}^{PV}(t_{srt,da}^{PV} + j\tau), \\ &\forall I_{step,da}^{PV,G} \in I_{step,da}^{PV}, \forall I_{step,da}^{PV} \in I_{step} \end{aligned} \tag{11}$$

2.1.2. Forecasted household demand modeling

A load profile depicts a household's electrical energy demand profile. We assume that the residences are equipped with various electrical appliances such as shiftable load, non-shiftable load, and etc. Since the energy consumption of a house is associated with the number of appliances that simultaneously draw energy, the mathematical model for the predicted energy can be expressed as follows:

$$\begin{aligned} &\left[\hat{E}_{FD,t+1}^{H_h}, \hat{E}_{FD,t+2}^{H_h}, \ldots, \hat{E}_{FD,t+I_{step}^{H_h}}^{H_h}\right] = \\ &\prod_{Model}^{H_h}\left(\left[\sum_{i=1}^{N_a} E_{D,t-T_k+1}^{H_h,A_i}, \ldots, \sum_{i=1}^{N_a} E_{D,t-1}^{H_h,A_i}, \sum_{i=1}^{N_a} E_{D,t}^{H_h,A_i}\right]\right) \\ &\forall t \in T_{hr}, \forall T_{hr} \in T, \forall t \in T_{mnt}, \forall T_{mnt} \in T, \forall t \in T_{snd}, \\ &\forall T_{snd} \in T, \forall h \in N_h, \forall H \in \mathbf{H}, \forall a \in N_a, \forall A \in \mathbf{A} \end{aligned} \tag{12}$$

where, $\prod_{Model}^{H_h}$ represents the Bi-LSTM model for energy demand forecasting and $\left[I_{step,d}^{H_h}, I_{step,da}^{H_h}\right] \in I_{step}^{H_h}$. Similarly, $\left[\hat{E}_{FD,t+1}^{H_h}, \hat{E}_{FD,t+2}^{H_h}, \ldots, \hat{E}_{FD,t+I_{step}}^{H_h}\right]$ can be determined for $(H_1, H_2, H_3, \ldots, H_{N_h}) \in \mathbf{H}$. The following equations are used to determine the overall forecasted energy demand:

$$\hat{E}_{FD,sum,d}^{H_h} = \sum_{j=0}^{I_{step,d}^{H_h}} \hat{E}_{FD,t}^{H_h}(t_{srt,d}^{H_h} + j\tau), \forall I_{step,d}^{H_h} \in I_{step,d} \tag{13}$$

In the present day circumstances, the energy demand during PV generating and in the absence of PV generation can be derived as follows:

$$\hat{E}_{FD,sum,d}^{H_h,G} = \sum_{j=0}^{I_{step,d}^{PV,G}} \hat{E}_{FD,t}^{H_h}(t_{srt,d}^{PV} + j\tau), \quad \forall I_{step,d}^{PV,G} \in I_{step,d}^{PV}, \forall I_{step,d}^{PV} \in I_{step,d} \tag{14}$$

$$\hat{E}_{FD,sum,d}^{H_h,NG} = \sum_{j=0}^{I_{step,d}^{H_h,NG}} \hat{E}_{FD,t}^{H_h}(t_{end,d}^{PV} + j\tau), \quad \forall I_{step,d}^{H_h,NG} \in I_{step,d}^{H_h}, \forall I_{step,d}^{H_h} \in I_{step,d} \tag{15}$$

Under the following day scenario, the total energy consumption and the energy consumption during the presence of PV generation can be calculated as follows:

$$\hat{E}_{FD,sum,da}^{H_h} = \sum_{j=0}^{I_{step,da}^{H_h}} \hat{E}_{FG,t}^{H_h}(t_{srt,da}^{H_h} + j\tau), \quad \forall I_{step,da}^{H_h} \in I_{step} \tag{16}$$

$$\hat{E}_{FD,sum,da}^{H_h,G} = \sum_{j=0}^{I_{step,da}^{PV,G}} \hat{E}_{FD,t}^{H_h}(t_{srt,da}^{PV} + j\tau), \quad \forall I_{step,da}^{PV,G} \in I_{step,da}^{PV}, \forall I_{step,da}^{PV} \in I_{step,da} \tag{17}$$

2.2. Tariff setting

The per unit charge of the electricity depends on the usage allowance. In the proposed system, we consider the grid energy usage allowance on a daily basis. According to the Korea Electric Power Corporation (KEPCO) website [36], the daily maximum allowance can be determined from the monthly allowance. The maximum daily allowance of the grid energy for each house is calculated as follows:

$$\hat{E}_{d,Th_i}^{grid,H_h} = \frac{\hat{E}_{m,Th_i}^{grid,H_h}}{N_{day}} \tag{18}$$

Therefore, the flat tariff setting can be defined as follows:

$$T_{t,d}^{H} = \begin{cases} T_{t,d}^{th_0}, & \text{if } \hat{E}_{d,Th_0}^{grid,H_h} < \hat{E}_{sum,d}^{grid,H_h} \le \hat{E}_{d,Th_1}^{grid,H_h} \\ T_{t,d}^{th_1}, & \text{if } \hat{E}_{d,Th_1}^{grid,H_h} < \hat{E}_{sum,d}^{grid,H_h} \le \hat{E}_{d,Th_2}^{grid,H_h} \\ \vdots & \\ T_{t,d}^{th_{n-1}}, & \text{if } \hat{E}_{d,Th_{n-1}}^{grid,H_h} < \hat{E}_{sum,d}^{grid,H_h} \le \hat{E}_{d,Th_n}^{grid,H_h} \end{cases} \tag{19}$$

2.3. Optimal capacity determination of PV-CESS

We assume multiple PV-CESS integrated systems for a residential community. To determine the optimal size of the PV-CESS, we consider the PV and battery properties and the individual energy consumption profile. For the PV capacity, we consider the average daily generation hour and efficiency of the PV panel. The following formulas are used to determine the total maximum daily power usage and total maximum grid energy allowance for the residences under the community.

$$\hat{E}_{sum,d}^{H_{all},max} = \sum_{h=1}^{N_h} \hat{E}_{sum,d}^{H_h,max} \times \eta_{DF}^{H_h,max} \tag{20}$$

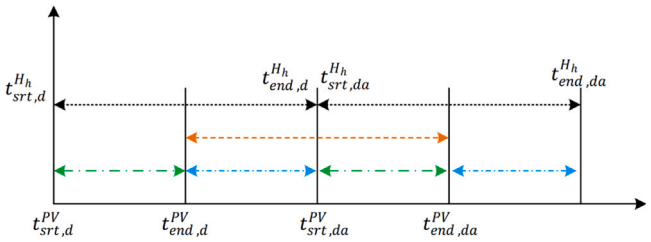

Fig. 3. Time frame for optimal operation.

$$\hat{E}_{d,Th_i}^{grid,H_{all}} = \sum_{h=1}^{N_h} \hat{E}_{d,Th_i}^{grid,H_h} \tag{21}$$

The PV capacity can be defined as follows:

$$\hat{E}_{d,Cap}^{PV,G} = \frac{\left(\hat{E}_{sum,d}^{H_{all},max} - \hat{E}_{d,Th_i}^{grid,H_{all}}\right)}{\eta_{GP}^{PV} \times \eta_{eff}^{PV}} \tag{22}$$

The thermal and electrical properties of different batteries are different. For example, LiFePO4 batteries can be continually discharged to a 100% depth of charge (DOD) without any long-term effects. However, to enhance the battery lifetime, discharging to 80% is recommended [37]. Moreover, the charging and discharging efficiencies of the inverter must be considered [38]. Therefore, the maximum PV generation and sum of minimum energy demand during the PV generation can be calculated as

$$\hat{E}_{sum,G}^{PV,max} = \sum_{g=1}^{N_{pv}} \hat{E}_{sum,d}^{PV_g,G} \times \eta_{GF}^{PV_g,max} \tag{23}$$

$$\hat{E}_{I_{step,d}^{PV,G},d}^{H_h,min} = \sum_{j=0}^{I_{step,d}^{PV,G}} \hat{E}_{D,t}^{H_h,min}(t_{srt,d}^{PV} + j\tau), \quad \forall I_{step,d}^{PV,G} \in I_{step,d}^{PV}, \forall I_{step,d}^{PV} \in I_{step,d} \tag{24}$$

$$\hat{E}_{I_{step,d}^{PV,G},d}^{H,min} = \sum_{h=1}^{N_h} \hat{E}_{I_{step,d}^{PV,G},d}^{H_h,min} \times \eta_{DF}^{H_h,min} \tag{25}$$

Since we have considered the backup capacity factor, the capacity of the CESS is defined as follows:

$$\hat{E}_{d,Cap}^{CESS} = \eta_{CF}^{CESS} \times \left(\hat{E}_{sum,G}^{PV,max} - \hat{E}_{I_{step,d}^{PV,G},d}^{H,min}\right) \tag{26}$$

Algorithm 1 Clustering algorithm

```
Function CLUSTERING (E_H, T, lb, ub, N_c^h, P = [])
S ← Sum(P)
if lb <= (S − T) <= ub then
    if len(P) = N_c^h then
        C ← P
    end if
else if S ≥ T then
    return
end if
for every number i do
    n = E_H[i]
    R = E_H[i + 1 :]
    Function CLUSTERING (R, T, lb, ub, N_c^h, P + [n])
end for
end
```

3. Optimization and clustering approach

The objective of the proposed system is to minimize the daily electricity costs through the integration of PV-CESS. Hence, we assume

Algorithm 2 Optimization and clustering algorithm during PV generation

Input: $\hat{E}^{PV,G}_{FG,sum,d}$, $\hat{E}^{CESS}_{nd,PV}$, η_{opt}, N_j, lr, lb, ub, N^h_c, and N_c
Output:
if $\hat{E}^{PV,G}_{FG,sum,D} > \hat{E}^{CESS}_{nd,PV}$ **then**
  Compute Eq. (29).
  $Z \leftarrow \hat{E}^{PV,G}_{sur}$
  $Y \leftarrow \sum_{g=1}^{N_g} \hat{E}^{PV,G}_{sur,g}$
  while $j > N_j$ **do**
    $x \leftarrow j \times lr$
    $X \leftarrow \sum_{h=1}^{N_h} \hat{E}^{H_h,G}_{FD,sum,D} \times F(x) \times \eta_{opt}$
    if $(Y - (lb - j)) < X < (Y + (ub - j))$ **then**
      $O_H \leftarrow X$
      break
    end if
    $j \leftarrow j + 1$
  end while
  $lr \leftarrow lr \times j$
  for every iteration k **do**
    Function **CLUSTERING** $(O_H, Z[0], lb + k, ub - k, N^h_c)$
  end for
  C_1 1^{st} cluster of house for 1^{st} PV
  $O_H \leftarrow (O_H - C_1)$
  for every iteration k **do**
    Function **CLUSTERING** $(O_H, Z[N_c - 1], lb + k, ub - k, N^h_c)$
  end for
  C_n $N_c th$ cluster of house for $N_c th$ PV
  $O_H \leftarrow (O_H - C_{N_c})$
else
  Compute Eq. (31).
  $Z \leftarrow 0$
end if
end

that the key approach to decreasing the daily electricity cost is to maximize the self-consumption of the PV power. The surplus PV energy must be distributed among the houses because the proposed scheme operates under the constraint that the energy feed to the utility grid is not reimbursed. Similarly, the CESS energy must be distributed among the houses by considering the day-ahead demand and generation, given that it can store the maximum PV energy during generation.

For optimization and clustering, every 24 h time horizon is divided into two operation periods: (a) during PV generation and (b) during no PV generation, which differ in terms of parameters such as the predicted energy consumption, PV generation, DOD, and initial SOE. Fig. 3 shows the proposed time-frame structure that is applied in the system. Since the charging and discharging processes in energy storage cannot be performed simultaneously, the surplus PV energy and CESS energy are expected to be used in the PV generation period and no PV generation period, respectively, based on the constraints and dependencies of the PV-CESS. The operational process can be described as follows:

3.1. Clustering of houses during PV generation

The objective of this operation is to distribute the surplus PV energy among the houses during the operational period of PV generation. Hence, we consider the forecasted PV generation, forecasted demand during PV generation, and initial SOE of the CESS at the operational time. The initial SOE and energy needed (i.e., PV energy) to completely charge each CESS can be defined as follows:

$$\hat{E}^{CESS}_{Ini,SOE}(t^{PV}_{srt}) = \left(\hat{E}^{CESS}_{Ini,20\%} + \hat{E}^{CESS}_{Pri,SOE}(t^{PV}_{srt})\right) \tag{27}$$

$$\hat{E}^{CESS}_{nd,PV} = \left(\hat{E}^{CESS}_{d,Cap} - \hat{E}^{CESS}_{Ini,SOE}(t)\right) \tag{28}$$

Algorithm 3 Optimization and clustering algorithm during no PV generation

Input: $\hat{E}^{PV,NG}_{FG,sum,d}$, $\hat{E}^{CESS}_{nd,PV}$, η_{opt}, N_j, lr, lb, ub, N^h_c, and N_c
if Constraint (34) **then**
  if Constraint (35) **then**
    if Constraint (36) **then**
      Compute Eq. (37).
    else if Constraint (38) **then**
      Compute Eq. (39).
    end if
  else if Constraint (40) **then**
    if Constraint (41) **then**
      Compute Eq. (42).
    else if Constraint (43) **then**
      Compute Eq. (44).
    end if
  end if
  $Z \leftarrow \hat{E}^{CESS}_{DisA}$
  $Y \leftarrow \sum_{cess=1}^{N_{cess}} \hat{E}^{CESS}_{DisA}$
  while $j > N_j$ **do**
    $x \leftarrow j \times lr$
    $X \leftarrow \hat{E}^{H_h,NG}_{FD,sum,D} \times F(x) \times \eta_{opt}$
    if $(Y - (lb - j)) < X < (Y + (ub - j)$ **then**
      $O_H \leftarrow X$
      break
    end if
    $j \leftarrow j + 1$
  end while
  $lr \leftarrow lr \times j$
  for every iteration k **do**
    Function **CLUSTERING** $(O_H, Z[0], lb + k, ub - k, N^h_c)$
  end for
  C_1 1^{st} cluster of house for 1^{st} CESS
  $O_H \leftarrow (O_H - C_1)$
  for every iteration k **do**
    Function **CLUSTERING** $(O_H, Z[N_c - 1], lb + k, ub - k, N^h_c)$
  end for
  C_n $N_c th$ cluster of house for $N_c th$ CESS
  $O_H \leftarrow (O_H - C_{N_c})$
else
  $Z \leftarrow 0$
end if
end

Consider that the total forecasted PV energy generation is greater than amount of energy necessary for properly charging the CESSs; the surplus of PV energy and the final SOE of the CESS can be defined as follows:

$$\hat{E}^{PV,G}_{sur} = \left(\hat{E}^{PV,G}_{FG,sum,D} - \hat{E}^{CESS}_{nd,PV}\right) \tag{29}$$

$$\hat{E}^{CESS}_{Fin,SOE}(t^{PV}_{end}) = \left(\hat{E}^{CESS}_{Ini,SOE}(t^{PV}_{srt}) + \hat{E}^{CESS}_{nd,PV}\right) \tag{30}$$

On the other hand, the final SOE at time t^{PV}_{end} of CESS can be defined as follows:

$$\hat{E}^{CESS}_{Fin,SOE}(t^{PV}_{end}) = \left(\hat{E}^{CESS}_{Ini,SOE}(t^{PV}_{srt}) + \hat{E}^{PV,G}_{FG,sum,D}\right) \tag{31}$$

Finally, the following formulation represents the objective function for maximizing the utilization of surplus PV energy among clustered users:

$$min \left| \sum_{g=1}^{N_{pv}} \hat{E}^{PV_g,G}_{sur} - \sum_{h=1}^{N_h} \hat{E}^{H_h,G}_{FD,sum,D} \right| \tag{32}$$

Algorithm 1 explains how the cluster algorithm works. The optimization and clustering process during the PV generating period

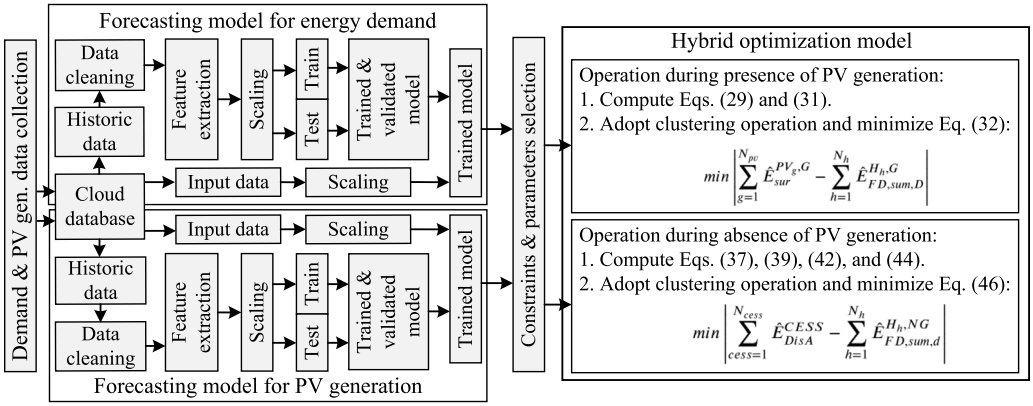

Fig. 4. Flow chart of the proposed approach.

is described by Algorithm 2. For accelerating optimization process, instead of a set learning rate, the $F(x) = tanh(x)$ function is applied.

3.2. Clustering of houses during no PV generation

The objective of clustering houses is to promote high-level coordination among them by considering the capacity and availability of CESS energy. Consequently, the maximum CESS energy can be supplied to the houses by considering the day-ahead PV generation and energy consumption during this operational period. Hence, we consider the forecasted PV generation, forecasted demand during no PV generation, and final SOE of the CESS at the eve of the operational period. In this regard, the usable energy of the CESS can be defined as follows:

$$\hat{E}^{CESS}_{Fin,uses}(t^{PV}_{end}) = \hat{E}^{CESS}_{Fin,SOE}(t^{PV}_{end}) \times \eta^{CESS}_{DOD} \times \eta^{CESS}_{eff} \tag{33}$$

The constraints of discharging the CESS can be defined as follows:

$$\hat{E}^{CESS}_{min,SOE} < \hat{E}^{CESS}_{Fin,SOE}(t^{PV}_{end}) \leq \hat{E}^{CESS}_{max,SOE} \tag{34}$$

Considering the day-ahead generation, the constraints and objective equation are derived for proper energy management. The CESS is completely discharged under higher day-ahead PV generation and lower day-ahead energy demand. The constraints and objective function can be defined as follows:

$$\sum_{g=1}^{N_{pv}} \hat{E}^{PV,G}_{FG,sum,da} \geq \sum_{g=1}^{N_{pv}} \hat{E}^{PV,G}_{FG,sum,d} \tag{35}$$

$$\sum_{h=1}^{N_h} \hat{E}^{H_h,NG}_{FD,sum,d} \geq \sum_{h=1}^{N_h} \hat{E}^{H_h,G}_{FD,sum,da} \tag{36}$$

$$\hat{E}^{CESS}_{DisA} = \hat{E}^{CESS}_{Fin,uses}(t^{PV}_{end}) \tag{37}$$

$$\sum_{h=1}^{N_h} \hat{E}^{H_h,NG}_{FD,sum,d} < \sum_{h=1}^{N_h} \hat{E}^{H_h,G}_{FD,sum,da} \tag{38}$$

$$\hat{E}^{CESS}_{DisA} = \hat{E}^{CESS}_{Fin,uses}(t^{PV}_{end}) \times \frac{\sum_{h=1}^{N_h} \hat{E}^{H_h,NG}_{FD,sum,d}}{\sum_{h=1}^{N_h} \hat{E}^{H_h,G}_{FD,sum,da}} \tag{39}$$

On the other hand, the discharge allowance are defined as follows:

$$\sum_{g=1}^{N_{pv}} \hat{E}^{PV,G}_{FG,sum,da} < \sum_{g=1}^{N_{pv}} \hat{E}^{PV,G}_{FG,sum,d} \tag{40}$$

$$\sum_{h=1}^{N_h} \hat{E}^{H_h,NG}_{FD,sum,d} \geq \sum_{h=1}^{N_h} \hat{E}^{H_h,G}_{FD,sum,da} \tag{41}$$

$$\hat{E}^{CESS}_{DisA} = \hat{E}^{CESS}_{Fin,uses}(t^{PV}_{end}) \times \frac{\sum_{h=1}^{N_h} \hat{E}^{H_h,G}_{FD,sum,da}}{\sum_{h=1}^{N_h} \hat{E}^{H_h,NG}_{FD,sum,d}} \tag{42}$$

$$\sum_{h=1}^{N_h} \hat{E}^{H_h,NG}_{FD,sum,d} < \sum_{h=1}^{N_h} \hat{E}^{H_h,G}_{FD,sum,da} \tag{43}$$

Table 1
Parameter initialization of PV system.

No.	$\hat{E}^{PV,G}_{d,Cap}$ (kW)	η^{PV}_{eff} (%)	$\eta^{PV,max}_{GF}$	η^{PV}_{GP} (h)
PV1	9.64	95.00	1.20	5.00
PV2	7.24	95.00	1.20	5.00
PV3	4.82	95.00	1.20	5.00

Table 2
Parameter initialization of CESS system.

No.	$\hat{E}^{CESS}_{d,Cap}$ (kWh)	η^{CESS}_{eff}	η^{CESS}_{DOD}	η^{CESS}_{CF}	$\hat{E}^{CESS}_{min,SOE}$
CESS1	41.02	90%	80%	1.20	20%
CESS2	30.77	90%	80%	1.20	20%
CESS3	20.51	90%	80%	1.20	20%

$$\hat{E}^{CESS}_{DisA} = \hat{E}^{CESS}_{Fin,uses}(t^{PV}_{end}) \times \frac{\sum_{h=1}^{N_h} \hat{E}^{H_h,NG}_{FD,sum,d}}{\sum_{h=1}^{N_h} \hat{E}^{H_h,G}_{FD,sum,da}} \tag{44}$$

The final SOE of the CESS at the end of the no PV generation period can be defined as follows:

$$\hat{E}^{CESS}_{Fin,SOE}(t^{H_h}_{end,d}) = \left(\hat{E}^{CESS}_{Fin,SOE}(t^{PV}_{end}) - \hat{E}^{CESS}_{DisA}\right) \tag{45}$$

where, $\hat{E}^{CESS}_{Fin,SOE}(t^{H_h}_{end,d}) = \hat{E}^{CESS}_{Ini,SOE}(t^{PV}_{srt,da})$ defines the initial SOE of CESS at the beginning of PV generation period in the next day. Finally, the following formulation represents the objective function for maximizing the usage of the CESS energy among clustered users:

$$min \left| \sum_{cess=1}^{N_{cess}} \hat{E}^{CESS}_{DisA} - \sum_{h=1}^{N_h} \hat{E}^{H_h,NG}_{FD,sum,d} \right| \tag{46}$$

Algorithm 3 presents the step-by-step procedure of the optimization and clustering operation during the PV generation period. In the case of optimization, the $F(x) = tanh(x)$ function is used instead of a fixed learning rate for accelerating the optimization process. Fig. 4 illustrates a comprehensive flowchart of the proposed approach, which comprises forecasting model and hybrid optimization model procedures.

4. Numerical experiment

We assume that each of the 15 houses has its own PV-ESS system to compensate its daily energy usage. In replacement of a individual PV-ESS, three PV-CESS are considered for evaluating the practical benefits of its energy usage. For this reason, the size and capacity of the CESS is determined based on the size of the individual PV-ESS while the individual capacity of the PV-ESS is determined based on the demand of the houses. Tables 1 and 2 present the parameters of each PV-CESS system. The PV capacity is determined considering the generation efficiency, maximum generation factor, and average generation hours.

Fig. 5. Energy demand scenarios of each house (a) *Day*1, (b) *Day*2, and (c) *Day*3.

Table 3
Hyperparameters for the forecasting model.

Hyperparameter	Model (Con.)	Model (Gen.)
Model neurons	64	30
Optimizer, Loss function	ADAM, Mean squared error	ADAM, Mean squared error
Learning rate	0.001	0.001
Number of hidden layers	1–3	1–3
Train, Validation, and Test data size	67.2%, 16.8%, 16%	67.2%, 16.8%, 16%
Epochs, Batch size	not fixed, 16	not fixed, 32
Patience	30	30

The charging and discharging capacity of each CESS is set as 90%, i.e., 10% energy is lost during charging and discharging. To enhance the battery health, the maximum DOD is set as 80%, i.e., the CESS can supply energy up to approximately 80% of its storage capacity. The initial state of charge (SOC) is 20% for each CESS. The daily plan is initiated from the beginning of the PV generation to ensure that the PV-generated energy can be appropriately utilized. In addition, the SOE level at the beginning and end of each operation is determined based on the forecasted constraints. Consequently, the CESS ensures the supply of energy to the consecutive operation.

Specifically, numerical experiments are performed to evaluate the performance of the proposed system. The numerical analysis involves the following aspects: (i) Evaluation of the accuracy of the forecasting model for PV generation and energy consumption; (ii) Evaluation of the performance of hybrid optimization algorithm; (iii) Cost comparison between the individual PV-ESS and PV-CESS based systems; and (iv) Accumulative cost comparison between the individual PV-ESS and CESS of the entire community.

We use six months' real energy demand and PV generation data of different houses. The data are extracted in 15 min intervals, leading to a total of 96 data samples for a single day. The daily time frame is divided into two categories, as shown in Fig. 3. Since we aim to solve a real-time problem, we consider the actual tariff plan offered by KEPCO. Python programming is performed to design and execute the proposed forecasting model and hybrid optimization algorithm. The device specifications are as follows: HP Z8 G4 Workstation with 256 GB of RAM and Intel® X®(R) Gold 5222 CPU @ 3.80 GHz 3.79 GHz processors.

To evaluate its feasibility, we test the proposed system in three scenarios:

1. Scenario 1 (Day 1): The forecasted energy demand for the ongoing day is lower than the predicted energy demand for the following day, but the forecasted PV generation for the ongoing day is higher than the predicted value for the following day.
2. Scenario 2 (Day 2): The forecasted energy demand for the ongoing day is higher than the predicted energy demand for the following day, but the forecasted PV generation for the ongoing day is lower than the predicted value for the following day.

Table 4
Performance of the predictive model (Bi-LSTM).

KPI	H1	H2	H3	H4	H5	H6	H7	H8	H9	H10	H11	H12	H13	H14	H15
MAE (kW)	.0089	.0166	.0128	.0137	.0126	.0111	.0141	.0153	.0172	.0204	.0096	.0137	.0098	.0116	.0091
RMSE (kW)	.0137	.0357	.0211	.0222	.0209	.0179	.0219	.0193	.0221	.0427	.0146	.0166	.0141	.0180	.0115
MAPE (%)	12.79	22.78	11.32	12.21	11.29	7.22	17.80	14.43	10.94	29.57	15.72	14.65	10.27	7.61	11.33
R2	0.86	0.83	0.84	0.90	0.85	0.87	0.86	0.75	0.89	0.88	0.80	0.81	0.81	0.87	0.59

3. Scenario 3 (Day 3): The forecasted energy demand for the ongoing day is almost equal to the predicted energy demand for the following day, but the forecasted PV generation for the following day is considerably smaller than the predicted PV generation for the ongoing day.

4.1. Predictive model performance

To drive the constraints and dependencies of the proposed energy management algorithm, we use the real-time energy demand of 15 houses and PV generation data of three PV systems to predict the day-ahead energy consumption and generation. Since we have considered the PV panels under the residential community, the pattern of solar irradiance are similar. Consequently, the same predictive model is used for all PV system. By adjusting the hyperparameter values, we have utilized the Bi-LSTM model to predict both energy generation and consumption. For each house, we employed a distinct Bi-LSTM model. Consequently, the number of epochs varies depending on the kind of house. Furthermore, we adapted "patience" to determine the minimum number of training epochs without progress before terminating. Table 3 illustrates the optimal hyperparameter values. The performance evaluation metrics of the proposed multistep forecasting algorithm are presented in Table 4. We consider multiple performance metrics such as the mean absolute error (MAE), root mean squared error (RMSE), mean absolute percentage error (MAPE), and R-squared (R2) to evaluate the prediction accuracy of the predictive model. Smaller values of the MAE, RMSE, and MAPE correspond to a superior predictive model. Larger R2 values represent a superior model performance. Models for $H1$ and $H10$ show low (i.e., .0089) and high prediction errors (i.e., .0204) in terms of the MAE, respectively, and models for $H15$ and $H10$ show the lowest (i.e., .0115) and highest (i.e., .0427) prediction errors in terms of the RMSE, respectively. The minimum and maximum MAPE correspond to models $H6$ and $H10$, respectively. All the predictive models show the standard R2 score, except $H15$. The performance metrics of the predictive PV generation model assessment are MAE: 0.71 W, RMSE: 1.26 W, MAPE: 16.42%, and R2: 0.99, which are suggestive of the satisfactory performance of the model.

4.2. Individual energy demand scenario

Fig. 5(a)–(c) illustrates the energy demand scenario of each house on three consecutive days. Those figures present the sum of the daily actual and forecasted energy demands. The differences of actual and predicted demand of each house indicates the predictive model performance. For certain homes, the predicted demand exceeds the actual demand, while for others, the predicted demand is lower than the actual value. Consequently, the variation between the total of a community's actual and predicted energy consumption is negligible. Moreover, we compute the average forecasting demand for optimal operation. Those figures also indicate the amount of energy consumption that exceeds the maximum daily grid energy allowance. The negative proportion of this demand represents the residential demand in excess of the grid's maximum limit. These findings assist in determining the daily cost of electricity for a specific tariff.

4.3. Clustering analysis

The houses have been grouped into three distinct categories to maximize the self consumption of daily PV-generated energy and CESS energy. First cluster operation is carried out at the beginning of PV generation, with forecasted PV generation and energy consumption constraints throughout PV generation period. Similarly, the second cluster operation is executed at the end of PV generation, taking into account the forecasted energy consumption in the absence of PV power generation. The first and second clusters are used to represent the excess PV generation energy distribution and CESS energy distribution among the houses, respectively. The clustering results of three consecutive days are shown in different figures. In the case of the first cluster, the X and Y axes refer to the excess PV energy and house demand, respectively. In the case of the second cluster, the X axis represents the usable CESS energy. To ensure the optimal solution, the clusters of PV1 and CESS1 are determined in advance owing to the high capacity of the PV and CESS. Similarly, the remaining clusters are determined for each case which is presented in the Algorithms. The houses under every cluster are different. For better perception, the amount of energy associated with the houses is presented in large text along with the house number. The clusters indicate that the excess PV energy of the PV panels can mitigate the house demand under that cluster. Similarly, the usable CESS energy can mitigate the house demand under that cluster. Thus the hybrid optimization algorithm can maximize the usage of the PV and CESS energy.

4.4. PV and CESS operations

The whole process, consisting of two separate optimal operations, is combined to reduce the daily power cost of the PV-ESS by maximizing the PV-energy utilization. The energy usage plan of each time horizon depends on the forecasted constraints. However, the results are presented in different tables, including the energy flow scenario, predicted PV generation, initial SOE of CESS, amount of energy needed to charge the CESS, clustered house under CESS, amount of energy supply to each house, and final SOE of CESS. In the following subsections, the PV and CESS operating characteristics for three consecutive days are described.

4.4.1. Scenario 1 (Day1)

Tables 5 and 6 summarize the results of the optimal operation during the presence of PV generation period and the absence of PV generation period, respectively. The results show that the proposed optimization and clustering algorithm maximize the use of surplus PV energy and CESS energy. Table 5 indicates that the predicted generation of the PV is larger than the storage capacity of the CESS. Consequently, the surplus PV energy is distributed such that the possible clustered houses can maximize the surplus energy usage. The houses under the PV1 and PV2 clusters use all the corresponding surplus PV energy, whereas the houses under PV3 utilize .08 kWh less than the PV3 surplus energy.

The CESS allocates certain energy for the subsequent day since the day-ahead predicted generation is lower and day-ahead demand is higher than those for the ongoing day. The CESS energy is supplied to each cluster for maximizing the usage of the CESS energy in a similar manner during PV generation operation. In the case of the CESS, we consider 10.00% energy loss during discharging. The difference between the maximum usable CESS energy and sum of

Table 5
Energy flow scenario during PV generation period for Day 1.

Name	PV-CESS1 (kWh)					PV-CESS2 (kWh)					PV-CESS3 (kWh)				
$\hat{E}^{PV,G}_{FG,sum}$			47.06					36.60					26.14		
$\hat{E}^{PV,G}_{sur}$			13.71					11.59					9.49		
Clustered house	H3	H8	H9	H12	H14	H2	H5	H6	H10	H13	H1	H4	H7	H11	H15
$\hat{E}^{H_h,G}_{FD,sum,d}$	5.55	5.11	7.81	4.49	6.18	5.39	5.50	6.05	3.21	4.52	3.00	5.44	5.08	3.01	3.49
PV energy supply	2.61	2.41	3.67	2.11	2.91	2.53	1.51	2.13	2.58	2.84	1.41	1.41	1.64	2.38	2.57
Grid supply	2.94	2.70	4.14	2.38	3.27	2.86	3.99	3.92	0.63	1.68	1.59	4.03	3.44	0.63	0.92
$\hat{E}^{CESS}_{Fin,SOE}(t^{PV}_{end})$			40.69					30.52					20.34		

Table 6
Energy flow scenario during no PV generation period for Day 1.

Name	PV-CESS1 (kWh)					PV-CESS2 (kWh)					PV-CESS3 (kWh)				
Clustered house	H3	H5	H6	H9	H14	H4	H7	H8	H11	H12	H1	H2	H10	H13	H15
$\hat{E}^{H_h,NG}_{FD,sum,d}$	4.21	4.17	6.16	7.14	6.20	6.43	4.21	4.22	2.46	3.45	3.08	2.56	2.09	3.17	2.82
CESS energy supply	3.49	3.46	5.10	5.92	5.14	5.33	3.49	3.50	2.04	2.86	2.55	2.13	1.73	2.63	2.33
Grid supply	0.72	0.71	1.05	1.22	1.06	1.10	0.72	0.72	0.42	0.59	0.53	0.44	0.36	0.54	0.48
$\hat{E}^{CESS}_{Fin,SOE}(t^{H_h}_{end})$			14.25					10.81					7.30		

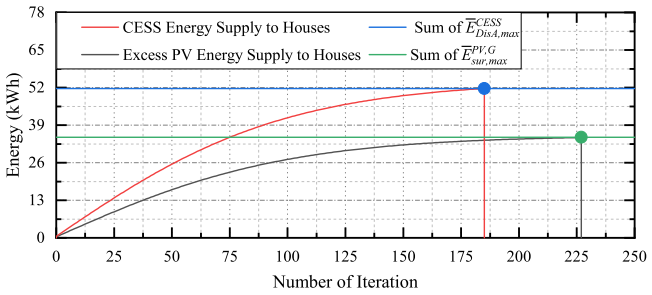

Fig. 6. Convergence graph for Scenario 1.

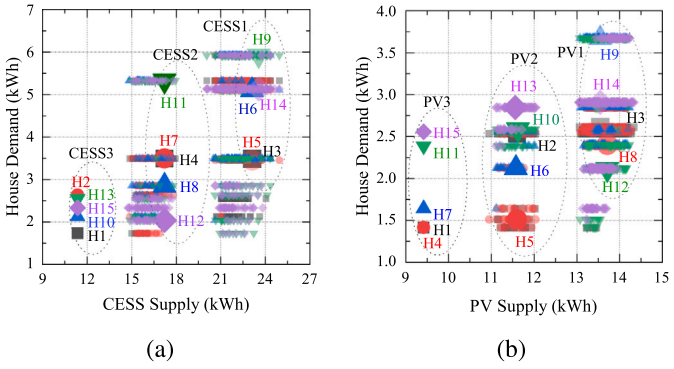

Fig. 7. Clustering results during (a) PV generation and (b) No PV generation for Scenario 1.

supplied energy under each cluster is 0.691, 0.526, and 0.361 kWh for CESS1–CESS3, respectively. Fig. 6 illustrate the convergence curve of the optimization algorithm, taking into account the surplus energy of 3 PV and dis-chargeable energy of 3 CESS. Additionally, the figure shows the maximum number of iterations to achieve the maximum utilization of the PV and CESS energy. Furthermore, Fig. 7 presents the clustering results during the presence PV and the absence of PV generation periods.

4.4.2. Scenario 2 (Day2)

The results of the hybrid optimization algorithm for Scenario 2 are presented in Tables 7 and 8 for the PV generation period and no PV generation period, respectively. The final SOE of Day 1 is considered as the initial SOE of Day 2 at the beginning of the Day 2 operation. After Day 1's operation period, the CESS stored more energy (i.e., high SOE level) due to lower forecasted PV generation and higher forecasted energy demand on Day 2, as shown in Table 7. In contrast, the CESS is completely charged during the operation PV generation (Day 2), and the surplus energy is supplied to the houses under each cluster. The results show that the houses under PV2 utilize the surplus energy completely, whereas the houses under PV1 use .01 kWh more energy and the houses under PV3 use .04 kWh less energy.

Since the day-ahead generation is higher and day-ahead energy demand is lower, the CESS is completely discharged for maximizing the PV self-consumption. Table 8 demonstrates that the final SOE of CESS1, CESS2, and CESS3 are 7.27 kWh, 6.33 kWh, and 3.59 kWh, respectively, representing the minimum SOE of each CESS. The CESS energy supplied to the clustered houses highlights that the proposed algorithm achieves the optimal solution. Fig. 8 depicts the convergence graph of both operations in the case of Day 2. Additionally, Fig. 9 shows the clustered result of with PV and no PV generation operation periods.

4.4.3. Scenario 3 (Day3)

In this case, the optimization and clustering performance under forecasted uncertainty is investigated to evaluate the feasibility and efficacy of the system. Similarly, the hybrid optimization algorithm requires Day 4 forecasted PV generation and energy demand data for every operation but we only consider three consecutive days of data. For this reason, we assume that the day-ahead predicted generation is lower than the ongoing generation (i.e., rainy day), and the day-ahead energy demand is equivalent to the ongoing demand. However, the optimization model is operated such that the houses can minimize the grid energy utilization. Tables 9 and 10 present the results obtained from the optimization and clustering algorithm. From the tables, it can be deduced that the proposed optimization and clustering approach preserves the expected level of energy in the CESS.

From the tables, the results highlight that the final SOE (Day 3)/initial SOE (Day 4) of the CESSs are higher than those in the previous two scenarios. The final SOE of CESS1, CESS2, and CESS3 are 23.16 kWh, 16.56 kWh, and 9.62 kWh, respectively. The convergence curve and clustering result of both operations are presented in Figs. 10 and 11. Fig. 10 demonstrate that the surplus energy and CESS energy are maximized in the 168th and 222nd iterations. The clustered result depict that the combination of houses in each cluster ensures the maximum utilization of the surplus energy and CESS energy. An optimal solution is obtained such that the consumers of each cluster are

Table 7
Energy flow scenario during PV generation period for Day 2.

Name	PV-CESS1 (kWh)					PV-CESS2 (kWh)					PV-CESS3 (kWh)				
$\hat{E}^{PV,G}_{FG,sum}$			34.92					27.16					19.40		
$\hat{E}^{PV,G}_{sur}$			8.47					7.45					6.36		
Clustered house	H3	H8	H9	H13	H15	H1	H4	H5	H7	H14	H2	H6	H10	H11	H12
$\hat{E}^{H_h,G}_{FD,sum,d}$	4.60	7.13	6.24	7.80	5.29	3.07	5.36	6.12	6.76	5.98	4.63	4.86	5.32	2.94	5.41
PV energy supply	1.26	1.95	1.70	2.13	1.44	0.84	1.46	1.67	1.85	1.63	1.26	1.33	1.45	0.80	1.48
Grid supply	3.35	5.19	4.54	5.67	3.84	2.23	3.89	4.45	4.92	4.35	3.37	3.54	3.86	2.14	3.93
$\hat{E}^{CESS}_{Fin,SOE}(t^{PV}_{end})$			40.69					30.52					20.34		

Table 8
Energy flow scenario during no PV generation period for Day 2.

Name	PV-CESS1 (kWh)					PV-CESS2 (kWh)					PV-CESS3 (kWh)				
Clustered house	H4	H6	H8	H9	H14	H5	H7	H12	H13	H15	H1	H2	H3	H10	H11
$\hat{E}^{H_h,NG}_{FD,sum,d}$	6.93	5.87	6.50	7.55	6.76	4.85	5.06	4.60	5.16	4.56	3.22	3.45	4.42	3.40	2.37
CESS energy supply	6.21	5.26	5.82	6.76	6.05	4.34	4.53	4.12	4.62	4.09	2.88	3.09	3.96	3.04	2.12
Grid supply	0.73	0.62	0.68	0.79	0.71	0.51	0.53	0.48	0.54	0.48	0.34	0.36	0.46	0.36	0.25
$\hat{E}^{CESS}_{Fin,SOE}(t^{H_h}_{end})$			7.27					6.33					3.59		

Table 9
Energy flow scenario during PV generation period for Day 3.

Name	PV-CESS1 (kWh)					PV-CESS2 (kWh)					PV-CESS3 (kWh)				
$\hat{E}^{PV,G}_{FG,sum}$			48.57					37.78					26.98		
$\hat{E}^{PV,G}_{sur}$			15.14					13.58					10.22		
Clustered house	H3	H5	H9	H14	H15	H2	H4	H6	H7	H11	H1	H8	H10	H12	H13
$\hat{E}^{H_h,G}_{FD,sum,d}$	6.17	6.14	7.02	5.26	3.56	3.72	4.75	5.14	4.90	6.75	2.76	4.89	2.97	4.26	4.02
PV energy supply	3.31	3.30	3.77	2.83	1.92	2.00	2.56	2.76	2.63	3.63	1.48	2.63	1.60	2.29	2.16
Grid supply	2.85	2.84	3.25	2.44	1.65	1.72	2.20	2.38	2.27	3.12	1.28	2.26	1.38	1.97	1.86
$\hat{E}^{CESS}_{Fin,SOE}(t^{PV}_{end})$			40.69					30.52					20.34		

Table 10
Energy flow scenario during no PV generation period for Day 3.

Name	PV-CESS1 (kWh)					PV-CESS2 (kWh)					PV-CESS3 (kWh)				
Clustered house	H4	H6	H8	H9	H14	H3	H5	H11	H12	H13	H1	H2	H7	H10	H15
$\hat{E}^{H_h,NG}_{FD,sum,d}$	4.34	4.82	4.16	5.22	5.27	3.77	4.04	3.67	3.79	3.96	2.60	2.95	3.66	2.51	3.47
CESS energy supply	2.59	2.87	2.48	3.11	3.14	2.25	2.41	2.19	2.26	2.36	1.55	1.76	2.18	1.49	2.07
Grid supply	1.75	1.95	1.68	2.11	2.13	1.52	1.63	1.48	1.53	1.60	1.05	1.19	1.48	1.01	1.40
$\hat{E}^{CESS}_{Fin,SOE}(t^{H_h}_{end})$			23.16					16.56					9.62		

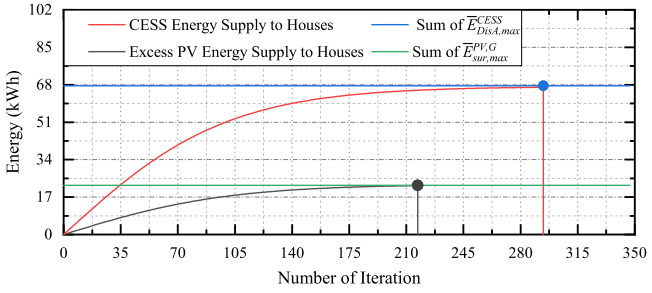

Fig. 8. Convergence graph for Scenario 2.

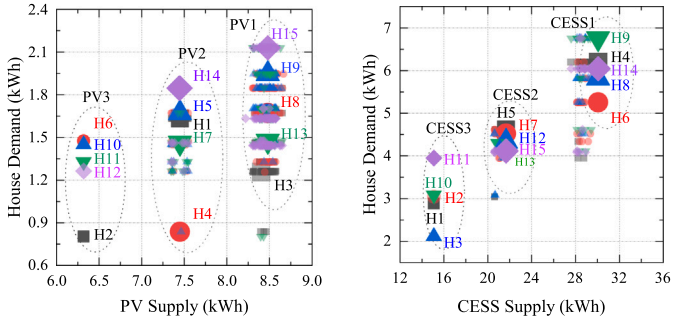

Fig. 9. Clustering results during (a) PV generation and (b) No PV generation for Scenario 2.

assigned to the same shared energy storage. The difference between the surplus energy and house demand in PV1, PV2, and PV3 are 0.01 kWh, 0.01 kWh, and 0.06 kWh, respectively. Similarly, CESS1 and CESS2 refrain from supplying energy to the houses by 1.24 kWh and 0.11 kWh, respectively, but CESS3 discharges 1.34 kWh more energy to the clustered houses.

4.4.4. State of CESS

Figs. 12, 13, and 14 depict the SOE and SOC state of CESS1, CESS2, and CESS3 throughout the period of three days according to the operational time period. The state of the SOE and SOC is continuously restricted by charging and discharging constraints. The graph displays the CESS's capacity to accurately coordinate the charging and

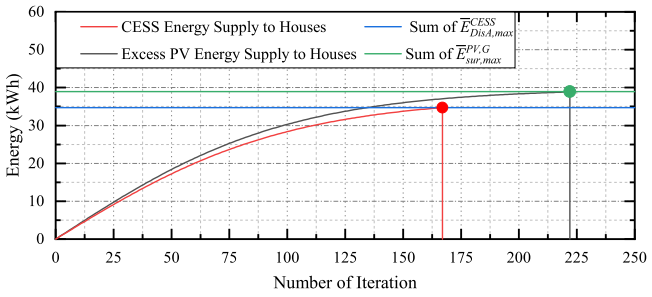

Fig. 10. Convergence graph for Scenario 3.

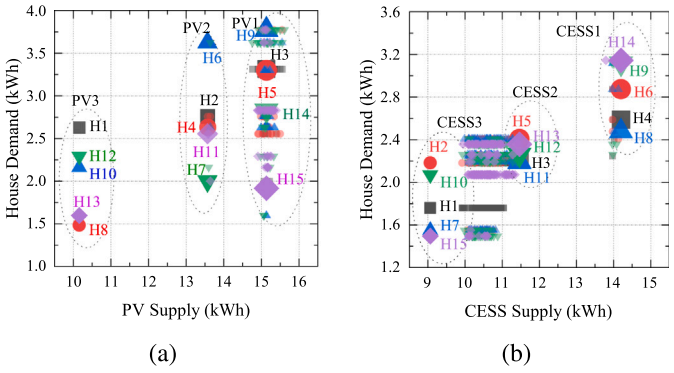

Fig. 11. Clustering results during (a) PV generation and (b) No PV generation for Scenario 3.

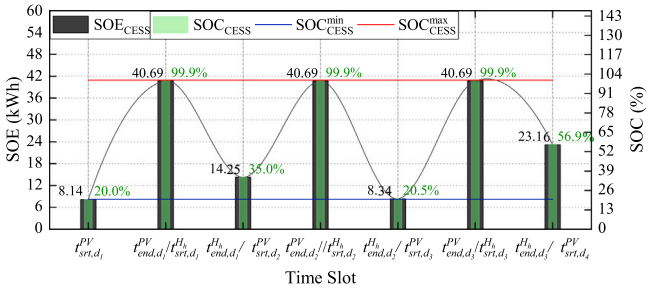

Fig. 12. SOE status of CESS1 for three consecutive days.

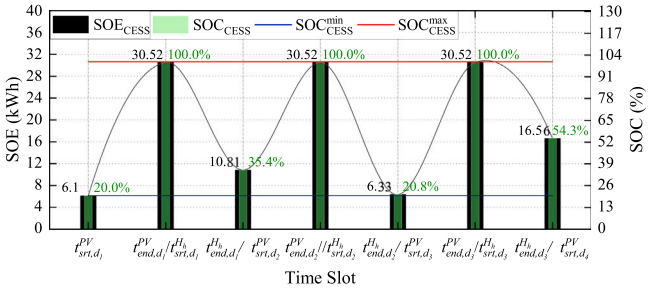

Fig. 13. SOE status of CESS2 for three consecutive days.

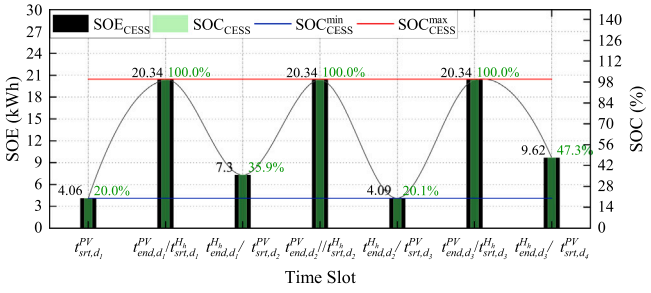

Fig. 14. SOE status of CESS3 for three consecutive days.

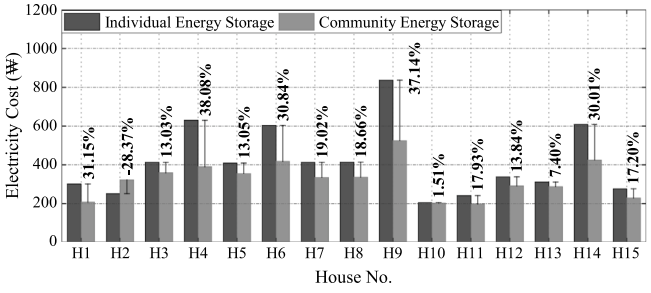

Fig. 15. Daily electricity cost comparison of each house under individual ESS and CESS for Scenario 1.

discharging process. When the PV energy generation is expected to be inadequate, the CESS stores energy for discharging the following day to ensure that the homes utilize the minimum amount of electricity from the utility grid. After Day 1 of operation, the SOC of the CESSs is approximately 15.00% higher than the initial state because the predicted day-ahead generations were 25.79% less than the current day generation volume. Figures illustrate that the three CESSs are in perfect condition while charging and discharging, with SOC states of 35.0%, 35.4%, and 35.9% respectively.

Similarly, the CESSs are fully discharged after Day 2 of operation because the day-ahead generation is nearly at its peak. According to the figures, the CESSs had SOC states of 20.5%, 20.8%, and 20.1%, respectively, indicating that they discharge flawlessly within the permissible boundaries. Furthermore, the CESSs preserve more energy after Day 3 of operation because of the comparatively small day-ahead PV generation. The SOC values of CESS1, CEES2, and CESS3 are 56.9%, 54.3%, and 47.3%, respectively, showing in the figures. Additionally, the SOC of each CESS changes as a consequence of the different amounts of energy that are charged and discharged during optimization and clustering operations.

4.5. Cost comparison

For the three consecutive days, we compute the daily electricity cost of each house under both individual PV-ESS and PV-CESS integrated systems. Because the energy fed to the utility grid will not be reimbursed, we assume that the energy demand of an individual house during PV generation is completely mitigated by the individual PV-ESS system's charging and discharging processes. Figs. 15, 16, and 17 illustrate the individual electricity cost for the three consecutive days. The results indicate that several houses have cost-saving percentages that are larger, smaller, or even negative.

These cost savings are attributable to the volume of energy consumption during PV generation. The proportion of cost savings increases as the energy consumption increases during periods of strong PV output. The negative percentage of cost savings indicates that the individual PV-ESS integrated system outperforms the PV-CESS because

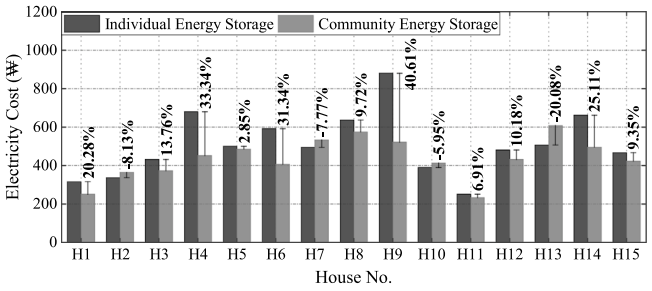

Fig. 16. Daily electricity cost comparison of each house under individual ESS and CESS for Scenario 2.

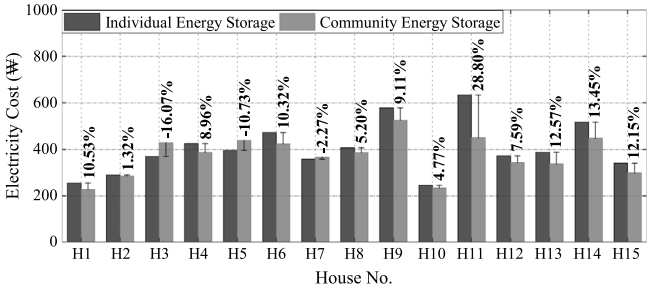

Fig. 17. Daily electricity cost comparison of each house under individual ESS and CESS for Scenario 3.

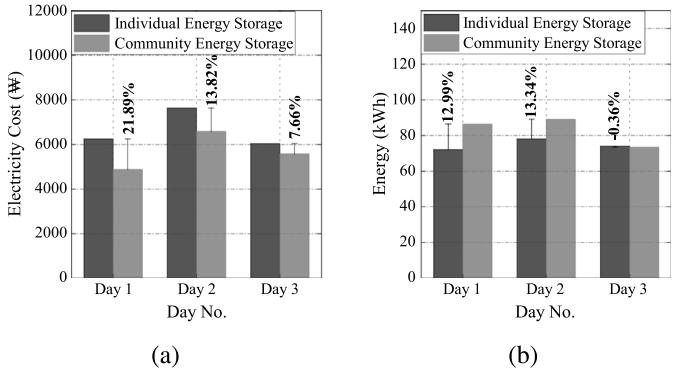

Fig. 18. Analysis of (a) overall cost and (b) PV-CESS energy utilization.

the houses consume significant energy during PV generation. The maximum and minimum percentages of daily power cost reduction with the PV-CESS integrated system are approximately 40.61% and −28.37% of H9 and H2, respectively. Unfavorable cost savings of a house on a day do not exclude it from benefiting from the PV-CESS system. Despite having the highest negative cost reduction on Day 1, H2 has a positive cost reduction on Day 3.

Additionally, we investigate the overall cost reduction under the PV-ESS and PV-CESS integrated systems, as shown in Fig. 18(a). The proposed PV-CESS system successfully minimizes a residential community's overall daily electricity costs. However, compared to that envisaged for Scenarios 1 and 2, the largest cost and lowest cost savings are 21.89% and 7.06%, respectively. Moreover, the overall percentages of daily PV energy self-consumption for the PV-ESS and PV-CESS are shown in Fig. 18(b). According to the proposed system, the day-ahead PV generating volume is the underlying cause of the highest and lowest percentages of self-consumption of PV energy under the PV-CESS system. Because the CESS reserves energy that is approximately 28.34% of its daily generation for the lowest day-ahead generation, the self-consumption of PV on Day 3 is the lowest (−0.36%). The negative sign represents the reduction of energy utilization of PV-CESS compared to individual PV-ESS.

5. Conclusion

This paper proposes an intelligent optimized energy management system for PV-CESS in a residential community considering the operational constraints and dependencies of the PV, CESS, and consumer demand. Without hampering the user satisfaction, the proposed system focuses on reliable forecasting, robust optimization, and clustering to decrease the daily electricity cost. The hybrid optimization algorithm ensured efficient energy management among the customer while the Bi-LSTM model maintained precise forecasting of both energy consumption and generation. The proposed system incorporates forecasting model in learning from prior experience with hybrid optimization model in exploring energy management to minimize the difference between PV energy generation and consumption.

Numerical analyses were conducted on different scenarios using real historical data to demonstrate the feasibility and effectiveness of the system. The numerical study shows that the CESS outperforms the individual ESS system in terms of lower electricity costs and increased self-consumption. In the three scenarios, the use of the CESS instead of the individual ESS results in daily power cost reductions of up to 21.89%, 13.81%, and 7.66% and daily PV-CESS energy utilization improvement of up to 12.99%, 13.34%, and −0.36%. Future work can be focused on enhancing the present formulation by including solar, wind, and other RESs with CESS through congestion management. The implementation of the proposed system at the hardware level is another promising research direction.

CRediT authorship contribution statement

Md. Morshed Alam: Conceptualization of this study, Methodology, Software, Writing – original draft. **Raihan Bin Mofidul:** Data curation, Writing – original draft. **Yeong Min Jang:** Supervision, Writing – review & editing.

Declaration of competing interest

The authors declare that they have no known competing financial interests or personal relationships that could have appeared to influence the work reported in this paper.

Data availability

Data will be made available on request.

Acknowledgments

This work was partly supported by the Technology Development Program of MSS [S3098815] and the MSIT (Ministry of Science and ICT), Korea, under the ITRC (Information Technology Research Center) support program (IITP-2022-2018-0-01396) supervised by the IITP(Institute for Information & Communications Technology Planning & Evaluation).

Appendix A

Before formulating day and day-ahead energy prediction, the following time step will be considered: (i) $I^{PV}_{step,d}$ and (ii) $I^{PV}_{step,da}$. The time

step will decide the input and output data size of the Bi-LSTM model. The ahead step of the forecasted energy is defined as follows:

$$I_{step}^{PV} = \frac{\left(t_{end,F}^{PV} - t_{srt,F}^{PV}\right)}{\tau}, \quad t_F^{PV} \in \left[t_{srt,F}^{PV}, t_{end,F}^{PV}\right], \\ \forall t_F^{PV} \in T_{hr}, \forall T_{hr} \in T, \forall t_F^{PV} \in T_{mnt}, \forall T_{mnt} \in T, \\ \forall t_F^{PV} \in T_{snd}, \forall T_{snd} \in T \forall \tau \in \tau_{hr}, \\ \forall \tau_{hr} \in \mathbf{I}, \forall \tau \in \tau_{mnt}, \forall \tau_{mnt} \in \mathbf{I}, \\ \forall \tau \in \tau_{snd}, \forall \tau_{snd} \in \mathbf{I} \tag{47}$$

where, τ defines the window size between two consecutive step and $\tau_{hr} \in (0, 23]$, $\tau_{mnt} \in (0, 1440)$, and $\tau_{snd} \in (0, 86\,400)$. Similarly, the day and day-ahead generation starting and ending time is $[t_{srt,d}^{PV}, t_{srt,da}^{PV}] \in t_{srt,F}$, $[t_{end,d}^{PV}, t_{end,da}^{PV}] \in t_{end,F}$, respectively. The daily optimal operations are divided into two distinct time periods: (i) when PV generation is present and (ii) when PV generation is absent. The time steps are represented by the following equations:

$$I_{step,d}^{PV} = \frac{\left(t_{end,d}^{PV} - t_{srt,d}^{PV}\right)}{\tau}, \quad \forall t_d^{PV} \in \left[t_{srt,d}^{PV}, t_{end,d}^{PV}\right], \\ \forall t_d^{PV} \in T_{hr}, \forall T_{hr} \in T, \forall t_d^{PV} \in T_{mnt}, \forall T_{mnt} \in T, \\ \forall t_d^{PV} \in T_{snd} \forall T_{snd} \in T \tag{48}$$

$$I_{step,d}^{PV,G} = \frac{\left(t_{end,d}^{PV,G} - t_{srt,d}^{PV,G}\right)}{\tau}, \quad \forall t_d^{PV,G} \in \left[t_{srt,d}^{PV,G}, t_{end,d}^{PV,G}\right] \\ \forall t_d^{PV,G} \in T_{hr}, \forall T_{hr} \in T, \forall t_d^{PV,G} \in T_{mnt}, \forall T_{mnt} \in T, \\ \forall t_d^{PV,G} \in T_{snd}, \forall T_{snd} \in T \tag{49}$$

No generation time is $t_{nG,d} \in (t_{end,d}, t_{srt,da})$ and $t_{nG,da} \in (t_{end,da}, t_{end,F})$. Similarly, the day-ahead time steps are formulated as follows:

$$I_{step,da}^{PV} = \frac{\left(t_{end,da}^{PV} - t_{srt,da}^{PV}\right)}{\tau}, \quad \forall t_{da}^{PV} \in \left[t_{srt,da}^{PV}, t_{end,da}^{PV}\right], \\ \forall t_{da}^{PV} \in T_{hr}, \forall T_{hr} \in T, \forall t_{da}^{PV} \in T_{mnt}, \forall T_{mnt} \in T, \\ \forall t_{da}^{PV} \in T_{snd} \forall T_{snd} \in T \tag{50}$$

$$I_{step,da}^{PV,G} = \frac{\left(t_{end,da}^{PV,G} - t_{srt,da}^{PV,G}\right)}{\tau}, \forall t_{da}^{PV,G} \in \left[t_{srt,da}^{PV,G}, t_{end,da}^{PV,G}\right] \\ \forall t_{da}^{PV,G} \in T_{hr}, \forall T_{hr} \in T, \forall t_{da}^{PV,G} \in T_{mnt}, \forall T_{mnt} \in T, \\ \forall t_{da}^{PV,G} \in T_{snd}, \forall T_{snd} \in T \tag{51}$$

Appendix B

Moreover, we need to compute distinct time steps for energy consumption regardless the PV energy prediction time steps. The underlying reason for formulating the independent time step for energy consumption is that the adjustment of both input and output size for the energy consumption prediction model (i.e., the Bi-LSTM model). The ahead step for the daily period is formulated as follows:

$$I_{step}^{H_h} = \frac{\left(t_{end,F}^{H_h} - t_{srt,F}^{H_h}\right)}{\tau}, \quad t_F^{H_h} \in \left[t_{srt,F}^{H_h}, t_{end,F}^{H_h}\right], \\ \forall t_F^{H_h} \in T_{hr}, \forall T_{hr} \in T, \forall t_F^{H_h} \in T_{mnt}, \forall T_{mnt} \in T, \\ \forall t_F^{H_h} \in T_{snd}, \forall T_{snd} \in T \forall \tau \in \tau_{hr}, \\ \forall \tau_{hr} \in \mathbf{I}, \forall \tau \in \tau_{mnt}, \forall \tau_{mnt} \in \mathbf{I}, \\ \forall \tau \in \tau_{snd}, \forall \tau_{snd} \in \mathbf{I} \tag{52}$$

$$I_{step,d}^{H_h} = \frac{\left(t_{end,d}^{H_h} - t_{srt,d}^{H_h}\right)}{\tau}, \quad \forall t_d^{H_h} \in \left[t_{srt,d}^{H_h}, t_{end,d}^{H_h}\right], \\ \forall t_d^{H_h} \in T_{hr}, \forall T_{hr} \in T, \forall t_d^{H_h} \in T_{mnt}, \forall T_{mnt} \in T, \\ \forall t_d^{H_h} \in T_{snd} \forall T_{snd} \in T \tag{53}$$

And the ahead step for the no generation period is formulated as follows:

$$I_{step,d}^{H_h,NG} = \frac{\left(t_{end,d}^{H_h} - t_{end,d}^{PV}\right)}{\tau}, \quad \left[\forall t_{end,d}^{PV}, \forall t_d^{H_h}\right] \in T_{hr}, \\ \forall T_{hr} \in T, \forall t_d^{H_h} \in T_{mnt}, \forall T_{mnt} \in T, \\ \forall t_d^{H_h} \in T_{snd} \forall T_{snd} \in T \tag{54}$$

The following equations are used to determine the time step for day-ahead energy demand:

$$I_{step,da}^{H_h} = \frac{\left(t_{end,da}^{H_h} - t_{srt,da}^{H_h}\right)}{\tau}, \forall t_{da}^{H_h} \in \left[t_{srt,da}^{H_h}, t_{end,da}^{H_h}\right], \\ \forall t_{da}^{H_h} \in T_{hr}, \forall T_{hr} \in T, \forall t_{da}^{H_h} \in T_{mnt}, \forall T_{mnt} \in T, \\ \forall t_{da}^{H_h} \in T_{snd} \forall T_{snd} \in T \tag{55}$$

References

[1] L. Luo, S.S. Abdulkareem, A. Rezvani, Reza M., Optimal scheduling of a renewable based microgrid considering photovoltaic system and battery energy storage under uncertainty, J. Energy Storage 28 (January) (2020) est.2020.101306.

[2] Seoul subsidizes installing new building-integrated solar panels, 2022, Accessed: Jul. 21, 2022. [Online]. Available: https://www.koreatimes.co.kr/www/nation/2022/05/371_328316.html.

[3] D. Parra, M. Gillott, S.A. Norman, G.S. Walker, Optimum community energy storagesystem for pv energy time-shift, Appl. Energy 137 (2015) 576–587.

[4] D. Parra, S.A. Norman, G.S. Walker, M. Gillott, Optimum community energy storagesystem for demand load shifting, Appl. Energy 174 (2016) 130–143.

[5] D. Parra, S.A. Norman, G.S. Walker, M. Gillott, Optimum community energystorage for renewable energy and demand load management, Appl. Energy 200 (2017) 358–369.

[6] A. Walker, S. Kwon, Analysis on impact of shared energy storage in residential community: Individual versus shared energy storage, Appl. Energy 282 (116172) (2021) 116172.

[7] S. van der Stelt, T. AlSkaif, W. van Sark, Techno-economic analysis of household and community energy storage for residential prosumers with smart appliances, Appl. Energy 209 (2018) 266–276.

[8] C. Wu, et al., A novel energy cooperation framework for community energy storage systems and prosumers, Int. J. Electr. Power Energy Syst. 134 (107428) (2022) 107428.

[9] H. Zhu, K. Ouahada, A distributed real-time control algorithm for energy storage sharing, Energy Build. 230 (110478) (2021) 110478.

[10] A. Taşcıkaraoğlu, Economic and operational benefits of energy storage sharing for a neighborhood of prosumers in a dynamic pricing environment, Sustain. Cities Soc. 38 (2018) 219–229.

[11] D. Zhao, H. Wang, J. Huang, X. Lin, Virtual energy storage sharing and CapacityAllocation, IEEE Trans. Smart Grid 11 (2) (2020) 1112–1123.

[12] J. Jo, J. Park, Demand-side management with shared energy storage system in smartgrid, IEEE Trans. Smart Grid 11 (5) (2020) 4466–4476.

[13] W. Zhang, W. Wei, L. Chen, B. Zheng, S. Mei, Service pricing and load dispatch of residential shared energy storage unit, Energy 202 (2020) 117543.

[14] L. Sun, J. Qiu, X. Han, X. Yin, Z.Y. Dong, Capacity and energy sharing platform withhybrid energy storage system: an example of hospitality industry, Appl. Energy 280 (2020) 115897.

[15] J. Liu, X. Chen, Y. Xiang, D. Huo, J. Liu, Optimal planning and investment benefit analysis of shared energy storage for electricity retailers, Int. J. Electr. Power Energy Syst. 126 (106561) (2021) 106561.

[16] S. Liu, et al., Operational optimization of a building-level integrated energy system considering additional potential benefits of energy storage, Prot. Control Mod. Power Syst. 6 (1) (2021).

[17] E. Telaretti, E.R. Sanseverino, M. Ippolito, S. Favuzza, G. Zizzo, A novel operating strategy for customer-side energy storages in presence of dynamic electricity prices, Intell. Ind. Syst. 1 (3) (2015) 233–244.

[18] F.J. Muñoz-Rodríguez, G. Jiménez-Castillo, J. de la Casa Hernández, J.D. Aguilar Peña, A new tool to analysing photovoltaic self-consumption systems with batteries, Renew. Energy 168 (2021) 1327–1343.

[19] J.C. Hernández, F. Sanchez-Sutil, F.J. Muñoz-Rodríguez, C.R. Baier, Optimal sizing and management strategy for PV household-prosumers with self-consumption/sufficiency enhancement and provision of frequency containment reserve, Appl. Energy 277 (115529) (2020) 115529.

[20] M. Gomez-Gonzalez, J.C. Hernandez, D. Vera, F. Jurado, Optimal sizing and power schedule in PV household-prosumers for improving PV self-consumption and providing frequency containment reserve, Energy (Oxf.) 191 (116554) (2020) 116554.

[21] C. Gallego-Castillo, M. Heleno, M. Victoria, Self-consumption for energy communities in Spain: A regional analysis under the new legal framework, Energy Policy 150 (112144) (2021) 112144.

[22] T. Weckesser, D.F. Dominković, E.M.V. Blomgren, A. Schledorn, H. Madsen, Renewable energy communities: Optimal sizing and distribution grid impact of photo-voltaics and battery storage, Appl. Energy 301 (117408) (2021) 117408.
[23] S.G. Varzaneh, A. Raziabadi, M. Hosseinzadeh, M.J. Sanjari, Optimal energy management for PV-integrated residential systems including energy storage system, IET Renew. Power Gener. 15 (1) (2021) 17–29.
[24] M.M. Alam, Y.M. Jang, Deep learning based optimal energy management framework for community energy storage system, ICT Express (2022).
[25] J. Choi, J.-I. Lee, I.-W. Lee, S.-W. Cha, Robust PV-BESS scheduling for a grid with incentive for forecast accuracy, IEEE Trans. Sustain. Energy 13 (1) (2022) 567–578.
[26] L. Moretti, S. Polimeni, L. Meraldi, P. Raboni, S. Leva, G. Manzolini, Assessing the impact of a two-layer predictive dispatch algorithm on design and operation of off-grid hybrid microgrids, Renew. Energy 143 (2019) 1439–1453.
[27] M.M. Alam, M.H. Rahman, M.F. Ahmed, M.Z. Chowdhury, Y.M. Jang, Deep learning based optimal energy management for photovoltaic and battery energy storage integrated home micro-grid system, Sci. Rep. 12 (1) (2022) 15133.
[28] S. Lilla, C. Orozco, A. Borghetti, F. Napolitano, Tossani F., Day-ahead scheduling of alocal energy community: an alternating direction method of multipliers approach, IEEE Trans. Power Syst. 35 (2) (2020) 1132–1142.
[29] A. Paudel, H.B. Gooi, Pricing in peer-to-peer energy trading using distributed optimization approach, in: IEEE Power & Energy Society General Meeting (PESGM) 2019, 2019, pp. 1–5.
[30] J. Iria, P. Scott, A. Attarha, Network-constrained bidding optimization strategy foraggregators of prosumers, Energy 207 (2020) 118266, http://dx.doi.org/10.1016/j.energy.2020.118266.
[31] M.J. Sanjari, H. Karami, Optimal control strategy of battery-integrated energy system considering load demand uncertainty, Energy (Oxf.) 210 (118525) (2020) 118525.
[32] S. Abedi, S. Kwon, Rolling-horizon optimization integrated with recurrent neural network-driven forecasting for residential battery energy storage operations, Int. J. Electr. Power Energy Syst. 145 (108589) (2023) 108589.
[33] S. Chapaloglou, et al., Smart energy management algorithm for load smoothing and peak shaving based on load forecasting of an island's power system, Appl. Energy 238 (2019) 627–642.
[34] S. Hochreiter, J. Schmidhuber, Long short-term memory, Neural Comput. 9 (8) (1997) 1735–1780.
[35] S. Srivastava, S. Lessmann, A comparative study of LSTM neural networks in forecasting day-ahead global horizontal irradiance with satellite data, Sol. Energy 162 (2018) 232–247.
[36] Rates Tables, Korea Electric Power Company, 2013, Accessed: Jan. 12, 2022. [Online]. Available: https://home.kepco.co.kr/kepco/EN/F/htmlView/ENFBHP00101.do{m}enuCd=EN060201.
[37] Battery storage 101 what-is-depth-of-discharge? 2022, Accessed: Jan. 24, 2022. [Online]. Available: https://www.solarips.com/blog/2021/january/battery-storage-101-what-is-depth-of-discharge-/j.
[38] C.-Y. Park, et al., Inverter efficiency analysis model based on solar power estimation using solar radiation, Processes (Basel) 8 (10) (2020) 1225.

Md. Morshed Alam has completed M.Sc. degree in Electronics Engineering from Kookmin University, South Korea. He is currently pursuing the Ph.D. degree in electronics engineering with Kookmin University. His research interests include Smart Grid, Renewable Energy, Internet of Energy, Deep Learning, and Machine Learning.
Email: mmorshed@ieee.org

Raihan Bin Mofidul is currently pursuing the M.Sc. degree in Electronics Engineering with, Kookmin University, South Korea. His research interests include Internet of Energy, Renewable Energy, and Deep Learning.
Email: raihanbinmofidul@ieee.org

Yeong Min Jang is the Professor at Kookmin University, Seoul, South Korea. His research interests include 5G/6G mobile communications, IoE, Smart Grid, and AI platform. He serves as the Editor-in-Chief of ICT Express. He has been the Director of the Internet of Energy Research Center since 2018.
Email: yjang@kookmin.ac.kr